The Plant Cell, Vol. 27: 1461–1476, May 2015, www.plantcell.org

The Control of *Arabidopsis thaliana* Growth by Cell Proliferation and Endoreplication Requires the F-Box Protein FBL17[OPEN]

Sandra Noir,[a] Katia Marrocco,[b] Kinda Masoud,[a] Alexis Thomann,[a] Andi Gusti,[a] Marta Bitrian,[a] Arp Schnittger,[a,1] and Pascal Genschik[a,b,2]

[a] Institut de Biologie Moléculaire des Plantes, CNRS, Unité Propre de Recherche 2357, Conventionné avec l'Université de Strasbourg, 67084 Strasbourg, France

[b] Institut de Biologie Intégrative des Plantes, Unité de Biochimie et Physiologie Moléculaire des Plantes, 34060 Montpellier, France

ORCID ID: 0000-0002-5666-2885 (S.N.)

A key step of the cell cycle is the entry into the DNA replication phase that typically commits cells to divide. However, little is known about the molecular mechanisms regulating this transition in plants. Here, we investigated the function of FBL17 (F BOX-LIKE17), an *Arabidopsis thaliana* F-box protein previously shown to govern the progression through the second mitosis during pollen development. Our work reveals that *FBL17* function is not restricted to gametogenesis. *FBL17* transcripts accumulate in both proliferating and postmitotic cell types of Arabidopsis plants. Loss of *FBL17* function drastically reduces plant growth by altering cell division activity in both shoot and root apical meristems. In *fbl17* mutant plants, DNA replication is severely impaired and endoreplication is fully suppressed. At the molecular level, lack of *FBL17* increases the stability of the CDK (CYCLIN-DEPENDENT KINASE) inhibitor KIP-RELATED PROTEIN2 known to switch off CDKA;1 kinase activity. Despite the strong inhibition of cell proliferation in *fbl17*, some cells are still able to enter S phase and eventually to divide, but they exhibit a strong DNA damage response and often missegregate chromosomes. Altogether, these data indicate that the F-box protein FBL17 acts as a master cell cycle regulator during the diploid sporophyte phase of the plant.

INTRODUCTION

The typical eukaryotic cell cycle is divided into four phases: the S phase (synthesis), during which the nuclear DNA becomes replicated; the M phase (mitosis), in which sister chromatids are separated and distributed to the newly forming daughter cells; and two gap phases, G1 and G2, that separate the S and M phases. The control of the G1-to-S transition is a key step in cell cycle regulation, since cells become typically committed to divide once they replicate their DNA (Nurse, 2000; Johnson and Skotheim, 2013). This step is tightly regulated in all eukaryotes by various mechanisms integrating intrinsic information such as nutrient status and hormonal signals with extrinsic, environmental conditions. The major control of the G1-to-S transition is exerted by CYCLIN-DEPENDENT KINASE (CDK) activities that are regulated at multiple levels and, in particular, by post-translational regulation of cyclin-dependent kinase inhibitors (CKIs; Murray, 2004). In both fungi and metazoans, it is well established that CKI degradation at the G1-to-S transition releases CDK activity, which in turn is required to enter S phase. For instance, in the budding yeast, the CKI called Sic1 can be phosphorylated by a G1 cyclin-CDK activity, and the phosphorylated Sic1 is then specifically recognized by the E3 ligase complex SCF^{Cdc4} (Skp1, Cdc53/CULLIN, and Cdc4, a WD40-type F-box protein), leading to its ubiquitylation and proteolysis (Schwob et al., 1994). In mammals, there are two classes of CKIs: the Ink4 (inhibitors of Cdk4) class and the Kip/Cip family (kinase inhibitory protein/CDK-interacting protein, including p21, p27, and p57). Similar to yeast, the mammalian $p27^{Kip1}$ protein becomes unstable when cells approach S phase, and its degradation requires phosphorylation by cyclin E-CDK2 activity in order to be recognized by the SCF^{SKP2} (SKP2 being a leucine-rich repeat-containing F-box protein; Starostina and Kipreos, 2012). Notably, besides SCF^{SKP2}, other E3 ligases are also required to fine-tune $p27^{Kip1}$ protein level during the cell cycle and development.

Over the last two decades, it became evident that the basic cell cycle machinery of plants shares a number of similarities with fungi or mammals but also exhibits some unique characteristics (Inzé and De Veylder, 2006; Harashima et al., 2013). However, despite its importance, little remains known about the molecular mechanisms of the G1-to-S transition in vascular plants (Genschik et al., 2014). The *Arabidopsis thaliana* Cdk1 homolog CDKA;1, which is required for both S-phase and mitosis entry (Nowack et al., 2012), operates independently of its dephosphorylation, indicating that the regulatory wiring of cell cycle regulation is different in plants versus yeast or metazoans (Dissmeyer et al., 2009). However, as in other kingdoms, plant CDKA;1 activity is negatively regulated by CKIs (Verkest et al., 2005b). So far, two classes of CKIs have been identified in

[1] Current address: University of Hamburg, Biozentrum Klein Flottbek, Department of Developmental Biology, Ohnhorststrasse 18, 22609 Hamburg, Germany.

[2] Address correspondence to pascal.genschik@ibmp-cnrs.unistra.fr.

The author responsible for distribution of materials integral to the findings presented in this article in accordance with the policy described in the Instructions for Authors (www.plantcell.org) is: Pascal Genschik (pascal.genschik@ibmp-cnrs.unistra.fr).

[OPEN]Articles can be viewed online without a subscription.

www.plantcell.org/cgi/doi/10.1105/tpc.114.135301

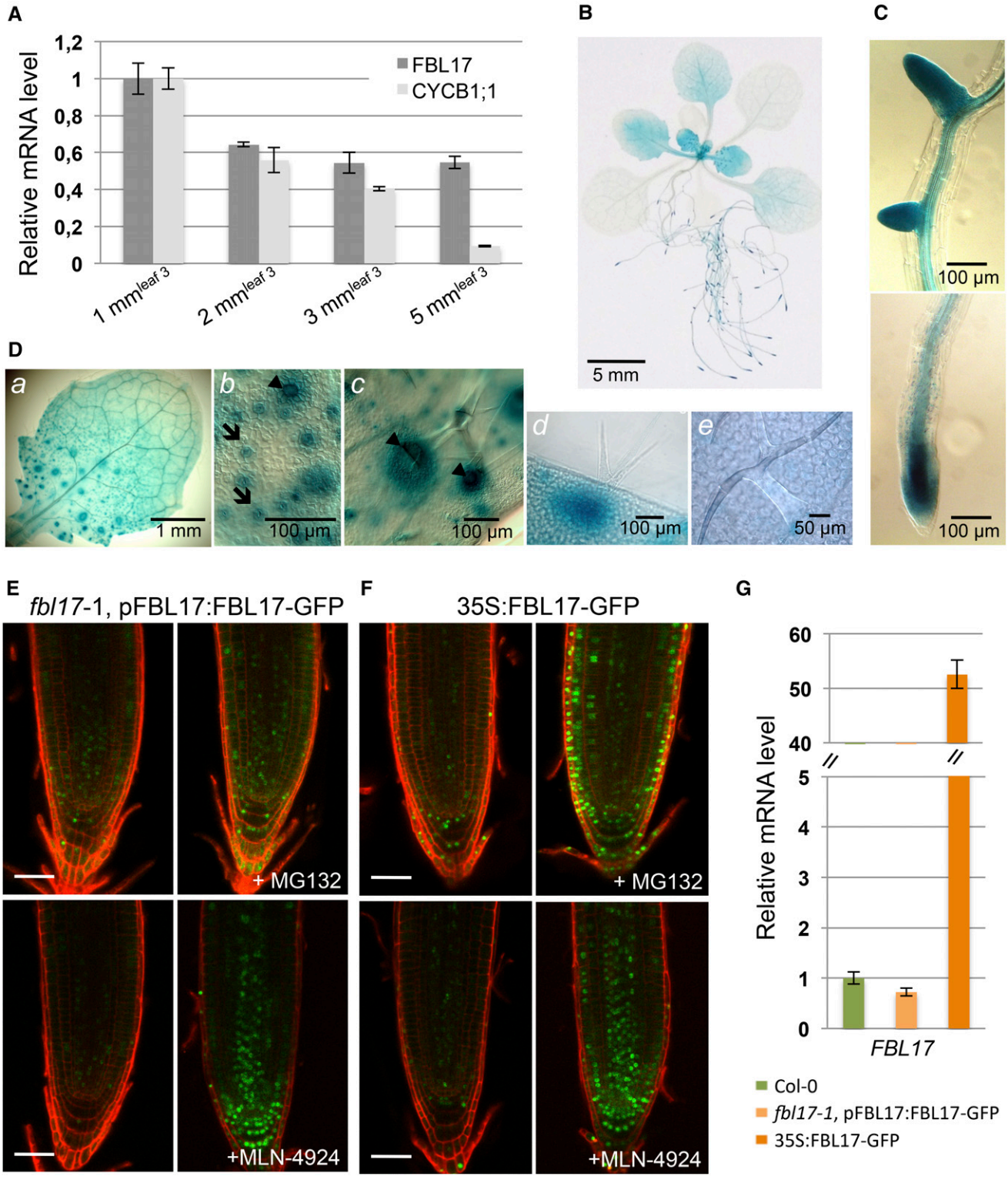

Figure 1. Expression of *FBL17* in Leaves and Roots.

(A) Relative expression levels of *CYCB1;1* and *FBL17* transcripts were determined by quantitative RT-PCR at different developmental stages of leaf 3 (i.e., 1-, 2-, 3-, and 5-mm leaf length). *CYCB1;1* expression is strictly related to dividing cells, while *FBL17* expression is maintained in more mature

Arabidopsis: (1) INTERACTOR/INHIBITOR OF CDKs, also called KIP-RELATED PROTEINs (ICK/KRPs; hereafter called KRPs), which show very restricted similarities to the mammalian Kip/Cip proteins (Torres Acosta et al., 2011); and (2) SIAMESE-RELATEDs, named after their founding member SIAMESE, which is phylogenetically even more distantly related to metazoan Kip/Cip proteins (Churchman et al., 2006; Peres et al., 2007). At the functional level, constitutive overexpression in transgenic plants of all KRPs tested so far could block both S and M phases, leading not only to growth retardation, including a reduction in cell number and organ size, but also to different developmental abnormalities, such as leaf serration (Verkest et al., 2005b). Therefore, protein levels of plant CKIs must be tightly regulated. Indeed, KRP2 proteasomal degradation depends on its CDK-dependent phosphorylation (Verkest et al., 2005a), a situation reminiscent of mammalian p27^{Kip1} SCF^{SKP2}-dependent degradation. However, the identity and role of ubiquitin E3 ligases destroying CKIs during plant development remain elusive.

Possible candidates for such ubiquitin E3 ligases have emerged recently from studies of Arabidopsis mutants deficient in cell division during gametogenesis. For instance, when RHF1a and RHF2a, two similar RING (REALLY INTERESTING NEW GENE)-finger proteins, are mutated in the *rhf1a rhf2a* double mutant, cell divisions during pollen and embryo sac development are severely impaired (Liu et al., 2008). Interestingly, a reduction in *KRP6* expression rescues in part the *rhf1a rhf2a* mutant phenotype, providing genetic evidence for a role of RHF E3s in KRP degradation during both male and female gametogenesis. Another player in cell cycle regulation during male gametogenesis is the F-box protein FBL17, as its corresponding loss-of-function mutants fail to undergo pollen mitosis II, which normally generates the two sperm cells in a mature pollen grain (Kim et al., 2008a; Gusti et al., 2009). Genetic evidence here also supports a function of FBL17 in KRP degradation during gametogenesis, as different KRP loss-of-function mutations suppressed, at least partially, the pollen-defect phenotype (Gusti et al., 2009; Zhao et al., 2012). However, whether *FBL17* functions beyond gametogenesis is unknown at present.

Here, we investigated the regulation and function of Arabidopsis *FBL17* during the diploid sporophyte life phase of the plant. While *FBL17* transcripts accumulate in both proliferating and postmitotic cell types, the protein is very unstable, being itself degraded in a proteasome-dependent manner. Loss of function of *FBL17* slows plant growth by decreasing cell proliferation and also suppresses endoreplication. Moreover, *fbl17* mutant plants show increased stability of the KRP2 protein, known to switch off CDKA;1 kinase activity, and resemble the *cdka;1* null mutant in many respects. However, the *fbl17* mutant cells that are able to enter S phase and divide exhibit mis-segregating chromosomes and a strong DNA-damage response. Overall, our results support a function of FBL17 as the main F-box protein involved in SCF-dependent regulation of the cell cycle at all stages of plant development.

RESULTS

FBL17 Is Expressed in Different Plant Organs and Is Regulated at the Posttranslational Level

Previous studies reported that *FBL17* is positively regulated by the transcription factor E2FA (Gusti et al., 2009) and repressed by RBR1 (RETINOBLASTOMA-RELATED1; Zhao et al., 2012), indicating that its expression is under cell cycle control, in particular during the progression toward S phase. To get more insight into the regulation of *FBL17*, we examined its expression in dividing cells versus postmitotic cells (Figure 1A). Arabidopsis leaves were harvested at different developmental stages, ranging from very young leaves with high cell division activity to fully expanded leaves, in which cell division activity is scarce and most cells are differentiated. As expected, the expression of *CYCB1;1* monitored by quantitative RT-PCR was correlated to cell division activity. By contrast, although *FBL17* expression was enriched in very young leaves, its transcript remained significantly expressed even in fully expanded leaves at a stage when the *CYCB1;1* transcript was downregulated. We next cloned an 868-bp fragment of the *FBL17* promoter sequence upstream of the *GUS* (β-*glucuronidase*) gene and selected 12 transgenic lines with a single reporter construct. Histochemical staining of the plants at different developmental stages confirmed that *FBL17* expression was enriched in proliferating tissues such as in young leaves, the primary root tip, and lateral

Figure 1. (continued).

leaves. The bar graph depicts expression level mean values of the indicated transcripts of one independent replicate (±SE of the technical triplicate). The experiment was repeated at least three times giving the same results.

(B) to **(D)** *FBL17* expression pattern revealed using *pFBL17:GUS* promoter-reporter fusion lines. Representative images show the histochemical localization of GUS activity in 20-d-old Arabidopsis plants stained for 2 h **(B)**; root primordia (top panel) and primary root apical meristem (bottom panel) **(C)**; and young leaf (*a*) exhibiting strong GUS activity in stomata cells (*b*, arrows) and trichome neighboring cells (*c* and *d*, arrowheads) in its dividing area, whereas such activity is absent in its differentiated area (*e*) **(D)**. Bars are as indicated.

(E) and **(F)** FBL17-GFP fusion proteins expressed under the control of its native promoter **(E)** or under the control of the constitutive CaMV 35S promoter **(F)** are stabilized in root cell nuclei treated for 6 h either with 100 μM MG132 (top panels) or with 25 μM MLN-4924 (bottom panels). Roots were counterstained with propidium iodide. Fluorescence images were obtained by confocal microscopy performed on roots of 7-d-old seedlings. Bars = 50 μm.

(G) Relative expression levels of *FBL17* transcripts in 10-d-old in vitro-grown plants of the indicated genotypes were determined by quantitative RT-PCR. The bar graph depicts expression level mean values of *FBL17* transcripts of one independent replicate (±SE of the technical triplicate). The experiment was repeated one time giving the same results.

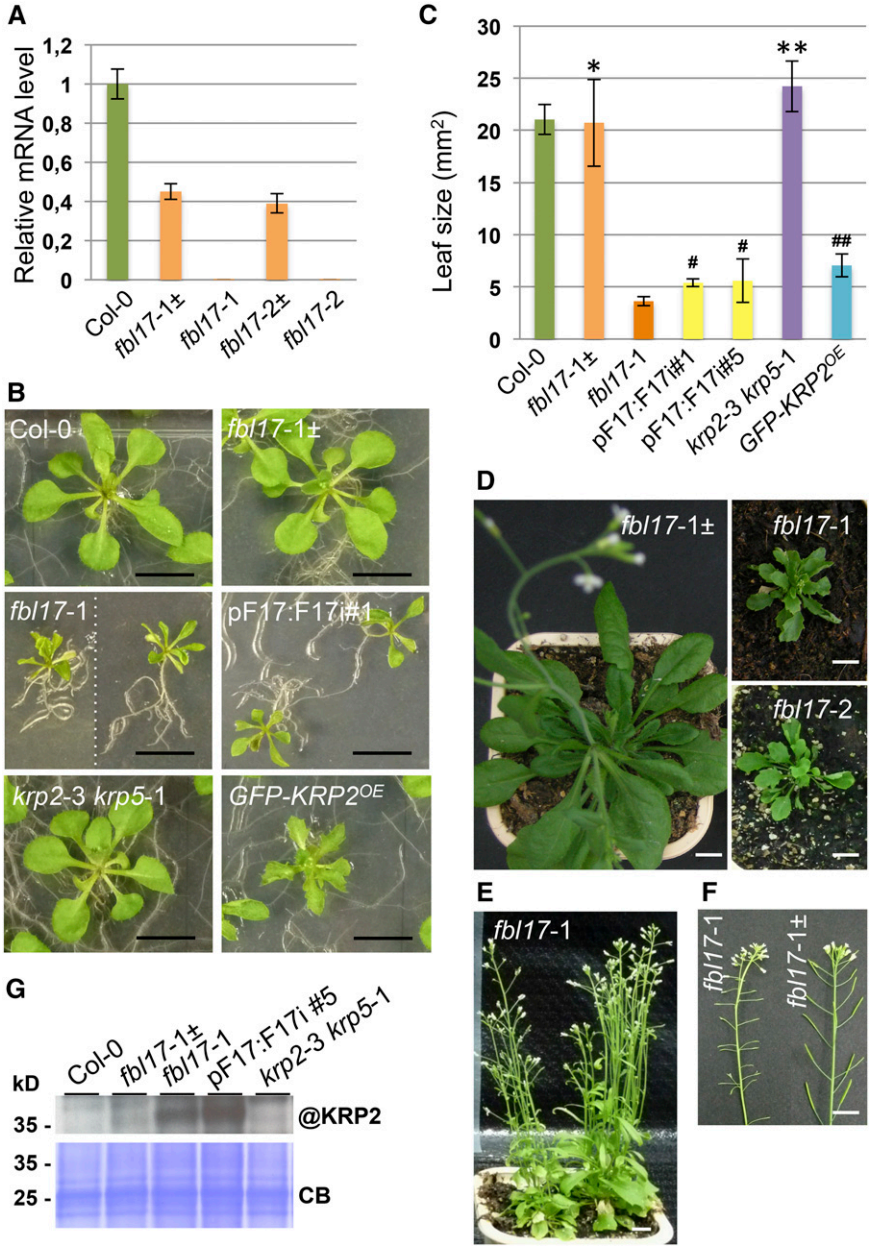

Figure 2. *fbl17* Mutants Show Severe Growth and Developmental Alterations and Overaccumulate the KRP2 Protein.

(A) Relative expression levels of *FBL17* transcripts were determined by quantitative RT-PCR in the two mutant lines *fbl17-1* and *fbl17-2* and compared with Col-0 and the respective *fbl17*± heterozygous mutant lines. The bar graph depicts expression level mean values of *FBL17* transcripts of one independent replicate (±SE of the technical triplicate). The experiment was repeated at least three times giving the same results. The locations of the quantitative PCR primers used to quantify *FBL17* transcript levels are indicated in Supplemental Figure 1.

(B) and **(C)** Using leaves 1 and 2 of 20-d-old seedlings of the indicated genotypes grown under in vitro conditions **(B)**, leaf areas were scored **(C)**. The bar graph depicts mean leaf areas (±SD) of five independent replicates based on five leaf pairs per genotype, except for *krp2-3 krp5-1*, for which three replicates were performed, and for pFBL17:FBL17i lines, for which two pairs were analyzed in two independent replicates. According to Student's *t* test, * and # indicate $P \geq 0.05$ and ** and ## indicate $P \leq 0.05$ when compared with Col-0 and *fbl17-1* bulked data, respectively. Bars in **(B)** = 1 cm.

(D) to **(F)** *fbl17-1* and *fbl17-2* mutants compared with *fbl17-1*± heterozygous plants grown on soil for 7 weeks **(D)** and 11 weeks **(E)**. *FBL17* loss-of-function mutants eventually flower and produce short siliques but are fully sterile **(F)**. Bars = 1 cm.

(G) Immunoblot analysis using an antibody against endogenous KRP2 (@KRP2) revealed strong accumulation of the protein in the *fbl17-1* null mutant and *pFBL17:FBL17i* lines. Coomassie blue staining was used as a loading control (CB). Three independent replicates were performed, yielding similar results.

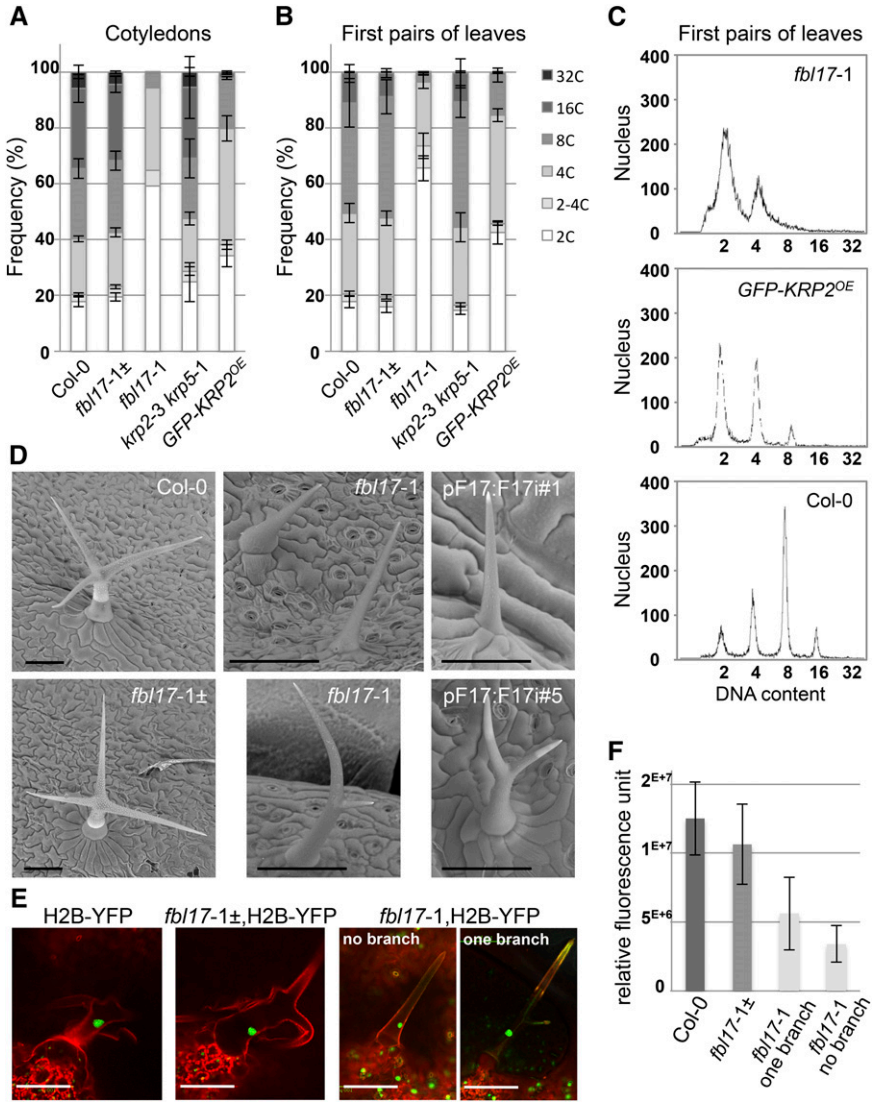

Figure 3. Endoreplication Is Severely Compromised in *fbl17* Mutants.

(A) and **(B)** Using flow cytometry analyses, nuclear DNA contents were measured from cells of cotyledons **(A)** and first pairs of leaves **(B)** of 20-d-old plants of the indicated genotype grown under in vitro conditions. The values represent average frequencies of the observed ploidy levels (or C, for chromatin value) of one experiment; error bars indicate SE. For each ploidy measurement, the analyses were performed on five samples of 2 to 3 bulked pairs of leaves/cotyledons per genotype, except for *fbl17-1* cotyledons, for which one sample of ~10 pairs was scored. Flow cytometry experiments were repeated three times with the leaf samples and two times with the cotyledons, giving similar results.

(C) A closer examination of the ploidy levels in *fbl17* mutants revealed broader 2C and 4C DNA content peaks, suggesting intermediary DNA content material in this genotype.

(D) Observations using scanning electron microscopy analyses show normal branched trichomes in wild-type and *fbl17-1*± heterozygous plants, while strong reductions in trichome growth and branching are observed in the *fbl17-1* mutants and RNAi lines. Images were taken from the adaxial surface of leaf 1 or 2 of 20-d-old plants of the indicated genotypes grown under in vitro conditions. Bars = 100 μm.

(E) and **(F)** The nuclear marker H2B fused to YFP was introduced into wild-type and *fbl17-1* mutant backgrounds. Based on confocal microscopy observations of trichome nuclei from leaf 1 or 2 of 13-d-old in vitro-grown H2B-YFP transgenic seedlings **(F)**, the average nucleus-integrated YFP intensity was quantified. The bar graph depicts average nucleus-integrated YFP intensity (±SE) from one replicate; the experiment was repeated once yielding similar results. For each replicate, ~10 trichomes were measured per genotype. Bars in **(E)** = 100 μm.

root meristems (Figures 1B and 1C). Notably, *GUS* expression was enriched in stomatal and trichome neighboring cells of the proliferating part of young leaves (Figure 1D). Although strongly reduced, *pFBL17:GUS* expression could still be detected in more mature leaves (Figure 1B).

Since F-box proteins are themselves unstable proteins degraded by the proteasome (Galan and Peter, 1999), we tested the accumulation of FBL17 protein. We engineered two different constructs, in which green fluorescent protein (GFP) was fused to the C terminus of FBL17 and expressed either under the control of 868 bp of the native promoter (pFBL17:FBL17-GFP) or under the control of the strong and constitutive cauliflower mosaic virus (CaMV) 35S promoter (35S:FBL17-GFP). Importantly, transgenic lines expressing the *pFBL17:FBL17-GFP* construct fully complemented the *fbl17-1* seed-abortion phenotype (Gusti et al., 2009), indicating that the FBL17-GFP fusion protein is functional.

Microscopy analyses revealed that the FBL17-GFP signal was faint and restricted to a few cells in the root meristem and was not significantly increased in *35S:FBL17-GFP* transgenic lines (Figures 1E and 1F, left panels), despite a high transcript accumulation of the transgene (Figure 1G), suggesting that the FBL17-GFP protein is unstable. Hence, after MG132 treatment, which blocks the activity of the proteasome, we observed a clear accumulation of FBL17-GFP in the nuclei of most cells at the root tip, and this effect was even stronger in *35S:FBL17-GFP* lines (Figures 1E and 1F, top panels). In this context, we investigated whether SCF-mediated ubiquitylation is required for FBL17 turnover by taking advantage of the MLN-4924 drug, a selective inhibitor of the NEDD8 (RUB1)-activating enzyme that inactivates Cullin-RING E3 ubiquitin ligases (CRLs) by blocking cullin neddylation in both mammals and plants (Hakenjos et al., 2011). Interestingly, upon MLN-4924 treatment, FBL17-GFP fusion proteins were efficiently stabilized in root tip cells (Figures 1E and 1F, bottom panels). These results reveal that FBL17 is regulated at the posttranslational level by a process requiring ubiquitylation by an SCF-type E3 ligase to restrict tightly the accumulation of the protein in plant cells.

The Very Few Viable *fbl17* Homozygous Mutants Are Severely Impaired in Growth and Remain Sterile

It was previously shown that homozygous mutant plants for the PSTAIRE kinase CDKA;1 could be recovered at low frequencies (Nowack et al., 2012). The presumed lack of KRP degradation in *FBL17* loss-of-function mutants should block CDKA;1 activity, suggesting that these mutants might exhibit a similar phenotype to *cdka;1* mutants. To test this hypothesis, we genotyped seed progeny of the two heterozygous *fbl17-1* and *fbl17-2* mutant alleles either grown in vitro or directly sown on soil. For both alleles, only ~1% homozygous mutant plants could be identified (Supplemental Table 1A); these mutants showed no detectable *FBL17* expression at the transcript level (Figure 2A; Supplemental Figure 1). These plants grew slowly compared with wild-type Columbia-0 (Col-0) or *fbl17-1*± heterozygous plants and produced leaves of smaller size (Figures 2B to 2D). The reduction in leaf size and the appearance of serrated leaves in *fbl17* null mutants is a phenotype also observed in KRP2-overexpressing plants (Figure 2B; De Veylder et al., 2001). By contrast, plants lacking the expression of KRPs exhibited leaves of slightly larger size, as illustrated for the *krp2-3 krp5-1* double mutant (Figures 2B and 2C). Despite their growth retardation phenotype, *fbl17* mutant plants were able to flower but remained fully sterile (Figures 2E and 2F). A closer examination by scanning electron microscopy revealed that, in these mutants, anthers and filaments remained smaller than those in the wild type and failed to produce pollen (Supplemental Figure 2A). This phenotype correlates with *FBL17* expression in these tissues (Supplemental Figure 2B).

As the isolation of *fbl17* homozygous mutants is very labor intensive due to their low frequency, we also sought to establish transgenic *FBL17* knockdown lines using RNA interference (RNAi). A hairpin of *FBL17* was expressed under the control of either the 35S promoter (35S:F17i lines) or the endogenous promoter (pF17:F17i lines; Supplemental Figure 3A). Over 20 T1 transformants for each construct were analyzed based on reduced growth, and most of them showed a reduction in *FBL17* expression (Supplemental Figure 3B). Several of these plants also presented serrated leaves and partial sterility. While this phenotype was still apparent in the T2 progeny, it could not be maintained throughout the generations due to the loss of *FBL17* gene silencing. Therefore, most of the analyses had to be performed with *fbl17* null alleles (Figure 2A) and, when possible, T2 RNAi lines with confirmed reduced *FBL17* expression (Figures 2B and 2C; Supplemental Figure 3).

FBL17 Loss of Function Leads to the Overaccumulation of KRP2 Protein and Blocks Endoreplication

The cyclin-dependent kinase inhibitor protein KRP2 inhibits CDKA;1 activity and was previously shown to be degraded by the proteasome (Verkest et al., 2005a). Its strong overexpression leads to reduced growth and the appearance of serrated leaves,

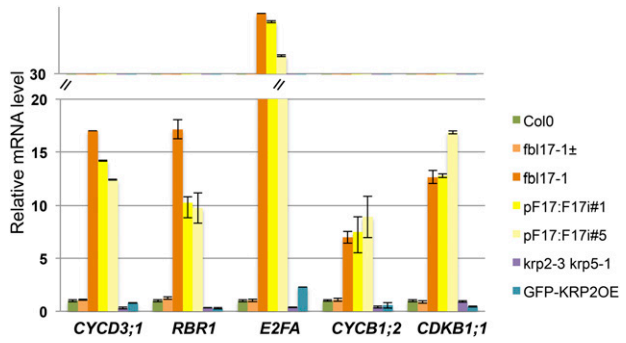

Figure 4. G1/S and G2/M Cell Cycle Genes Are Upregulated in *FBL17*-Deficient Lines.

Relative expression levels of *CYCD3;1*, *RBR1*, *E2FA*, *CYCB1;2*, and *CDKB1;1* transcripts in the first pair of leaves of 20-d-old in vitro-grown plants of the indicated genotype were determined by quantitative RT-PCR. The bar graph depicts expression level mean values of the indicated transcripts of one independent replicate (±SE of the technical triplicate). The experiment was repeated three times, giving the same results.

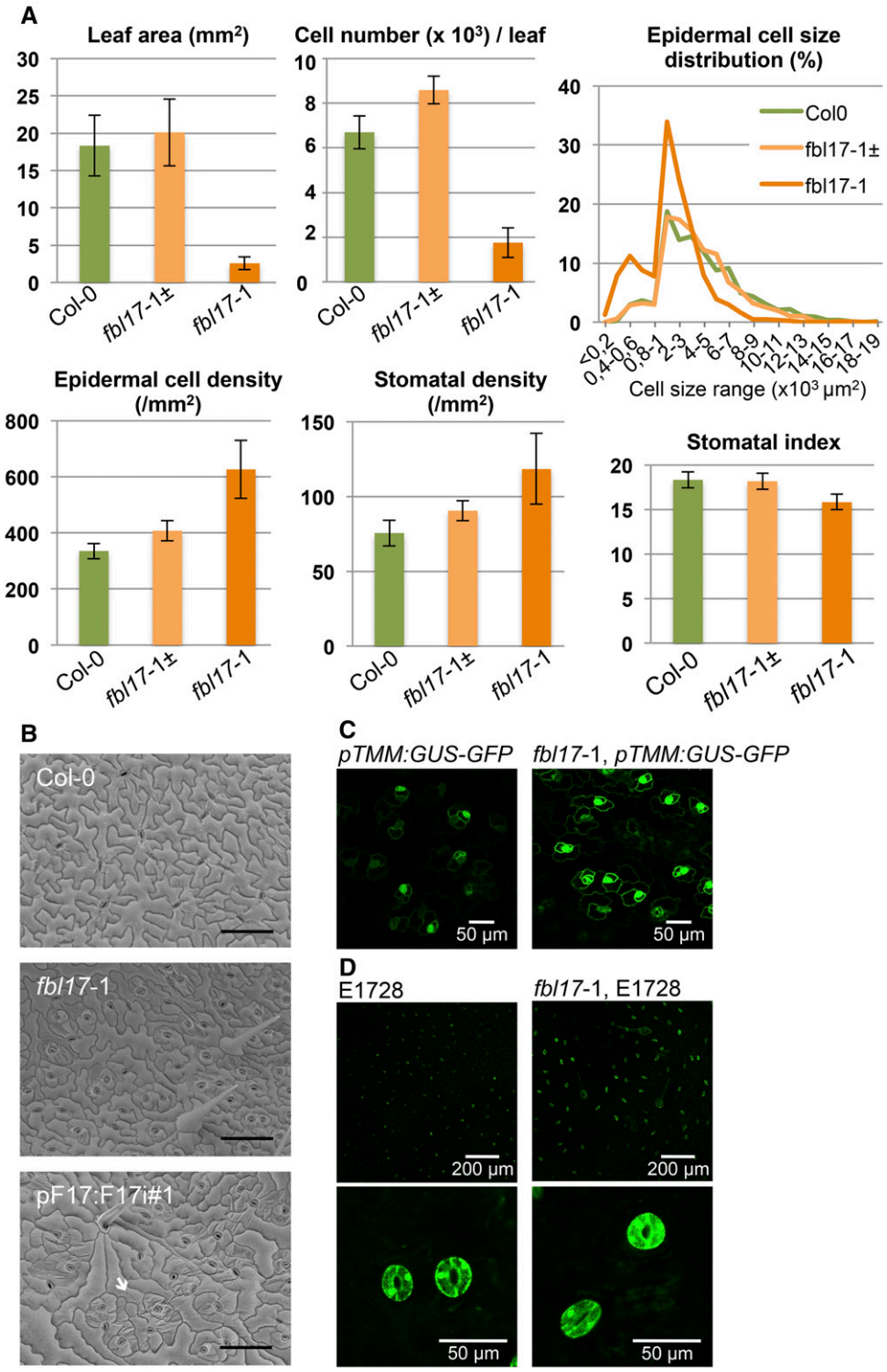

Figure 5. Cell Proliferation Is Strongly Impaired in *fbl17* Mutants.

(A) Leaf blade area, total cell number per leaf, epidermal cell size distribution, epidermal cell density, stomatal density, and stomatal index of the adaxial epidermis of the first true leaf pair of wild-type Col-0, *fbl17-1*± heterozygote, and *fbl17-1* homozygote mutant plants grown under in vitro conditions for 20 d. Shown are average data ± SE from one replicate. The experiment was repeated once, yielding similar results. For each replicate, five to eight pairs of leaves were measured per genotype.

a phenotype reminiscent of the *FBL17* loss-of-function phenotype, suggesting that KRP2 might be a target of the SCF^{FBL17} ubiquitin E3 ligase. Consistent with this idea, while endogenous KRP2 protein was hardly detected in wild-type plants because of its fast turnover, we observed its accumulation in both *fbl17-1* null and RNAi mutant lines (Figure 2G).

Strong accumulation of KRPs also suppresses endoreplication in Arabidopsis leaf cells (De Veylder et al., 2001; Schnittger et al., 2003); accordingly, we examined the ploidy levels in the cotyledons and the first pairs of leaves of 20-d-old wild-type and mutant plants by flow cytometry (Figures 3A to 3C). Interestingly, *FBL17* loss of function almost entirely suppressed nuclei of ploidy levels above 4C DNA content. This effect was even stronger than in plants overexpressing KRP2 from the CaMV 35S promoter (referred to as GFP-$KRP2^{OE}$). In addition, we noted that the 2C and 4C peaks in the *fbl17-1* mutant were not as sharp as observed in wild-type plants and that DNA with intermediate ploidy levels was detected (Figure 3C). Moreover, we analyzed trichomes of *fbl17* mutants, as these cells undergo multiple rounds of endoreplication, which is essential for their cell fate, cellular growth, and branching (Bramsiepe et al., 2010). While single cell trichomes in wild-type Arabidopsis usually have three to four branches, all trichomes in *fbl17-1* null and RNAi lines showed an altered level of branching (Figure 3D). These trichomes were very small in size and remained either not branched or only single-branched. To confirm that the *fbl17* mutant trichome phenotype correlates with a reduction in endoreplication, we introduced the chromatin marker H2B-YFP (histone 2B-yellow fluorescent protein) in these lines (Figure 3E). Fluorescence microscopy revealed that, as expected, wild-type plants expressing this marker display a significant amount of the nuclear H2B-YFP protein correlated with the increased amount of chromatin in the fully differentiated trichomes. By contrast, the fluorescence signal was reduced by half in *fbl17-1* single-branched trichomes and was even lower in nonbranched trichomes (Figure 3F), indicating that endoreplication was compromised in these mutant cells. From these data, we conclude that *FBL17* loss of function blocks entry into endoreplication, most likely by a failure in degrading KRP proteins.

Next, we wondered whether the phenotype of *fbl17* might essentially reflect the inability of the mutants to destroy KRP proteins. It was previously shown that several single *krp* mutants could at least partially rescue the pollen cell cycle arrest of *FBL17* loss of function (Gusti et al., 2009; Zhao et al., 2012). Thus, different combinations of mutations between *fbl17-1* and *krp* mutants were generated. Extensive genotyping of the progeny of the *fbl17-1* heterozygous mutation combined with multiple *krp* homozygous mutations revealed only a slight increase in the ratio of *fbl17-1* homozygous mutant plants (Supplemental Table 1B). However, we failed to identify *fbl17-1* plants for which growth retardation, leaf serration, or sterility was suppressed. As the Arabidopsis genome encodes seven KRP proteins, it is possible that the suppression of the *fbl17* phenotype requires the genetic removal of more KRPs, potentially all of them. It is also possible that KRPs are not the only substrates of SCF^{FBL17} and that the accumulation of other substrates, likely cell cycle regulatory proteins, could explain at least part of this phenotype.

FBL17 Loss of Function Dramatically Reduces Cell Proliferation in Leaves and Roots, but Cell Specification Is Maintained

To get more insight into the cellular defects of this mutant, we monitored by quantitative RT-PCR the expression of a selected set of cell cycle genes in the first pairs of leaves of 20-d-old wild-type and *fbl17-1* mutant lines (Figure 4). Interestingly, we found that the transcript levels of genes involved in S phase (such as *CYCD3;1*, *RBR1*, and *E2FA*) and genes involved in mitosis (such as cyclin *CYCB1;2* or *CDKB1;1*) were significantly increased in *fbl17-1* null and RNAi lines. The strong upregulation of these genes (especially the mitotic genes) was not expected, and this was also not observed in strong *KRP2*-overexpressing plants.

Next, we examined more precisely the adaxial lamina surface of the first pair of leaves of 20-d-old wild-type and *fbl17* mutant lines (Figure 5A). The reduction in leaf size correlates with a strong reduction in cell number, which is in agreement with *FBL17* acting as a positive regulator of cell proliferation. Scanning electron microscopy revealed that while wild-type leaf epidermis contains typical pavement cells with a jigsaw puzzle-like pattern and well-distributed mature stomata, this pattern was strongly altered in *FBL17* loss-of-function leaf epidermis (Figure 5B). In the *fbl17-1* mutants, the size of the pavement cells was highly variable. Unlike in the wild type, where the cell size follows a normal distribution, two peaks can be observed in the *fbl17-1* mutants with a high proportion of cells with very small area (i.e., <1000 μm^2; Figure 5A). Moreover, we observed in some epidermal areas an excess of stomata that eventually clustered (Figure 5B). Measurements on the adaxial leaf surfaces revealed that stomatal density (number of stomata per mm^2) was indeed increased in *fbl17-1* compared with wild-type leaves (Figure 5A). The *pTMM:GUS-GFP* marker (Nadeau and Sack, 2002) is primarily expressed in the stomatal cell lineage of

Figure 5. (continued).

(B) Scanning electron microscopy analyses showing adaxial epidermal cells of leaf 1 or 2 of 20-d-old wild-type Col-0, *fbl17-1* mutant, and the pF17:F17i#1 RNAi line. In both *fbl17* mutant lines, cell sizes appear very heterogeneous, with some areas exhibiting clusters of smaller cells including stomata (arrow). Bars = 100 μm.

(C) Expression of the stomatal cell lineage marker *pTMM:GUS-GFP* in adaxial epidermis of leaf 3 of 20-d-old wild-type and *fbl17-1* mutant plants. Bars are as indicated.

(D) Expression of the guard cell identity marker E1728 in adaxial epidermis of leaf 1 or 2 of 20-d-old wild-type and *fbl17-1* mutant plants. Bars are as indicated.

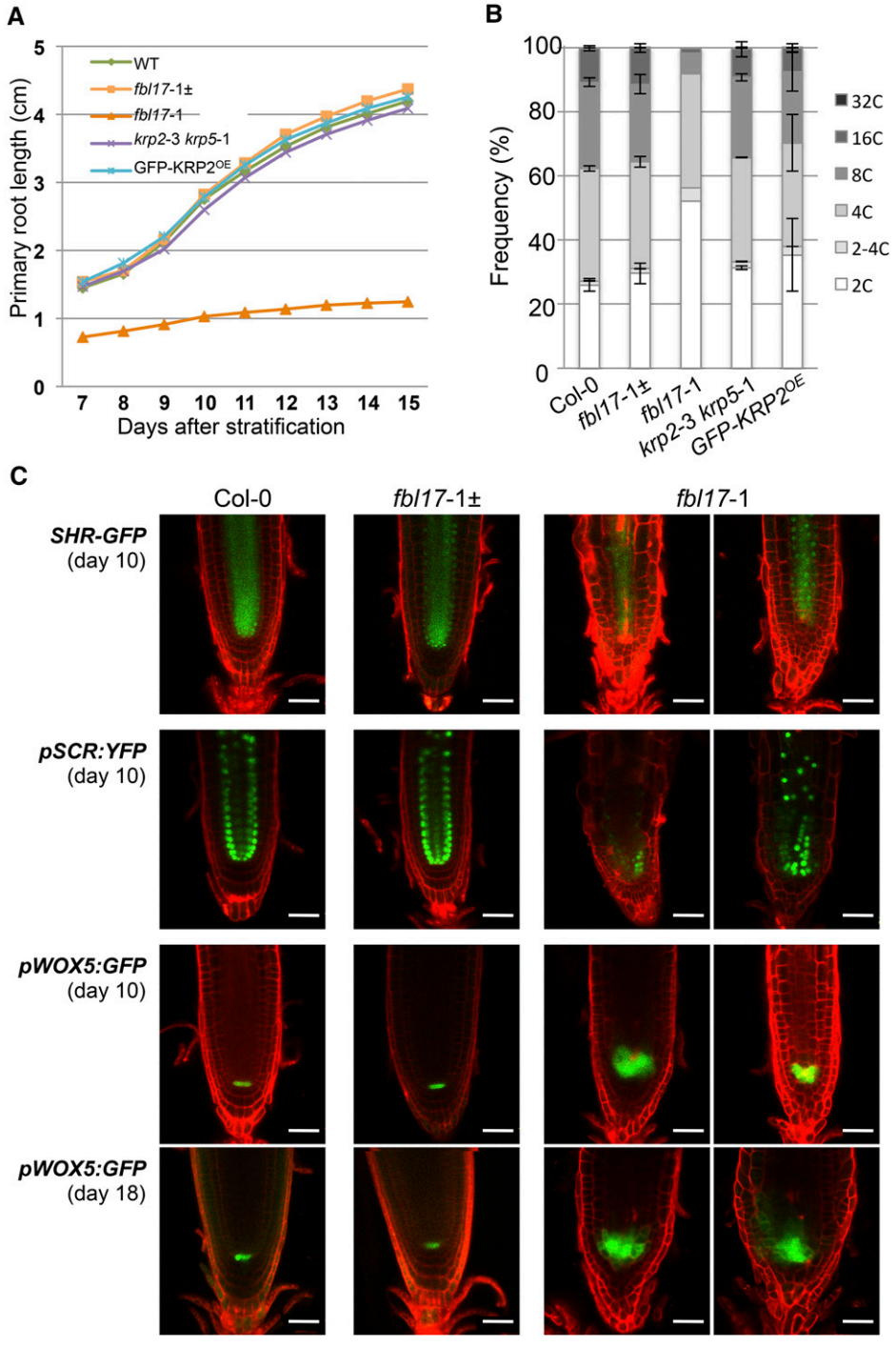

Figure 6. FBL17 Is Required to Maintain Meristem Activity but Not Cell Fate Specification.

(A) Kinetic analysis of the primary root elongation of the *fbl17-1* mutant. Seedlings of the indicated genotypes were grown on vertical plates, and digital images were daily taken for further root length measurements. For each replicate, the analyses were performed on 10 seedlings per genotype, except for *fbl17-1*, for which 5 to 10 primary roots were scored. Shown are data from one replicate. The experiment was repeated twice, yielding similar results.
(B) Using flow cytometry analyses, nuclear DNA contents were measured from root cells of 20-d-old plants of the indicated genotype grown under in vitro conditions. The values represent average frequencies of the observed ploidy (or C) levels of one experiment; error bars indicate SE. For each ploidy measurement, the analyses were performed on three samples of 2 to 4 bulked root systems per genotype, except for *fbl17-1*, for which one sample of 10 bulked root systems was scored. This experiment was repeated one time, yielding similar results.

developing epidermis, and a higher proportion of cells expressed this marker in the *fbl17* mutant background compared with the wild-type background (Figure 5C). However, taking into account that the overall epidermal cell density was also significantly increased in *fbl17-1*, the stomatal index [=stomatal density/(stomatal density + epidermal cell density)] was similar to that of the wild type or even slightly decreased (Figure 5A). In addition, once differentiated, stomatal cell fate in *fbl17-1* was not affected, as illustrated by stomata properly expressing the E1728 mature guard cell identity marker (Figure 5D).

We then investigated how *FBL17* loss of function affects primary root growth and development. As with the situation in leaves, primary root growth was severely compromised in the *fbl17-1* mutant (Figure 6A). In addition, endoreplication was drastically reduced in the root of the mutant line and, reminiscent of the observation in leaves, mutant root cells also exhibit a notable proportion of intermediary 2-4C DNA content (Figure 6B). A closer examination of mutant root tips revealed important cell disorganizations, with the early exhibition of differentiated hair cells at close proximity to the root meristem. However, the use of root-specific developmental markers indicates that cell identity was not affected, as the expression of genes for the GRAS-type transcription factors SHORT-ROOT (SHR) and SCARECROW (SCR), involved in root radial patterning and the maintenance of the root stem cell niche (Helariutta et al., 2000), could be detected (Figure 6C). Although we also clearly detected in the *fbl17-1* mutant the expression of *pWOX5:GFP* (in which *GFP* expression is driven by the promoter of *WUSCHEL-RELATED HOMEOBOX5*), a specific marker of the quiescent center (QC; Blilou et al., 2005), this signal was expanded (Figure 6C; Supplemental Figure 4A), suggesting supernumerary QC cells through either the division of QC cells or the adoption of QC fate by the neighboring cells. Similar results were obtained using the QC-specific promoter trap line QC46 (Sabatini et al., 1999; Supplemental Figure 4B). The enlarged QC might be a compensatory mechanism that attempts to maintain a functional stem cell niche in the light of a general reduction of cell division activity in *fbl17* mutants. Altogether, these data show that *FBL17* is required to maintain normal root growth through the regulation of root meristem activity.

FBL17 Loss of Function Impairs DNA Replication and Affects Proper Chromosome Segregation

Since we observed a strong upregulation of genes promoting both S phase and mitosis (Figure 4), we further characterized the cell cycle status of *fbl17* mutant cells in the root meristem. To detect cells actively replicating their DNA, we used 5-ethynyl-2′-deoxyuridine (EdU), a nucleoside analog of thymidine (Bass et al., 2014). Strikingly, despite the fact that the *fbl17* meristematic root zone appears short with fewer cells, quite a few of them showed EdU labeling, indicating that they entered into the S phase (Figure 7A). Moreover, in addition to the higher frequency of 2-4C DNA content observed in *fbl17* root cells compared with the wild type (Figure 6B), the late apparition of synchronized S phase in adjacent cells (Hayashi et al., 2013) of *fbl17* root tips during the EdU pulse-labeling experiment (Figure 7A, 5 and 8 h) points to a delay or even a blockage of DNA replication in those cells.

DNA replication stress activates cell cycle checkpoints and, in particular, induces the expression of the DNA damage kinase ATR (ataxia telangiectasia mutated and Rad3-related) (Culligan et al., 2004; Harper and Elledge, 2007; Cools and De Veylder, 2009) as well as the expression of another checkpoint kinase, WEE1, known to be induced upon the cessation of DNA replication (De Schutter et al., 2007). Interestingly, we could observe an upregulation of those two genes in *fbl17* mutants (Figure 7B). CYCB1;1, which is induced upon replication stress (Culligan et al., 2004, 2006), was also upregulated in the *fbl17* mutant. This was further confirmed using the *pCYCB1;1:Dbox-GUS* marker (Donnelly et al., 1999). While GUS expression was visible only in the shoot and root meristems as well as in young leaves of wild-type plants, the expression pattern of the transgene was broader in *fbl17-1* mutant plants exhibiting GUS staining also in more mature leaves, stems, and beyond the meristematic zone of the root (Supplemental Figure 5). This suggests that loss of *FBL17* function activates mechanisms of the G2-phase checkpoint regulation, which might result in some cell arrests in G2 phase. Moreover, we observed that BRCA1 (BREAST CANCER SUSCEPTIBILITY1), which responds to and is required for efficient DNA repair of double-strand breaks (Lafarge and Montané, 2003; Reidt et al., 2006), was also induced in the *fbl17* mutant (Figure 7B). Altogether, this suggests not only that normal DNA replication is compromised in the *fbl17* mutant but also that other events occurring during the G2 phase or mitosis are altered and could result in genome instability. To investigate this issue, we took advantage of the *fbl17-1* mutant line expressing the H2B-YFP chromatin marker. Imaging of chromatin showed that, in this mutant, the nuclear structure was overall altered, with small nuclei of abnormal shapes in comparison with the wild-type plant (Figure 7C; Supplemental Figure 6). Unlike yeast and animal cells, which, if failing to replicate properly their DNA do not enter into mitosis due to an efficient S-phase checkpoint, in the *fbl17-1* root meristem we were able to observe several

Figure 6. (continued).

(C) Expression patterns of root cell fate markers in wild-type and *fbl17-1* mutant backgrounds. Shown are confocal laser scanning images of primary root tips of 10- or 18-d-old (as indicated) seedlings expressing *SHR-GFP*, *pSCR:YFP*, and *pWOX5:GFP*. Roots were counterstained with propidium iodide (red signal). As shown previously (Welch et al., 2007), in wild-type Arabidopsis roots, SHR-GFP fusion proteins localize to cells of the stele and in the immediate-adjacent tissues to the stele, including the endodermis and the QC, while *pSCR:YFP* is expressed in endodermal cells and the QC. As SHR/SCR root functions are required for stem cell maintenance and cortex/endodermis differentiation, cell identity appears to be maintained in *fbl17-1* mutant root, while the radial patterning is slightly altered. Using the QC-specific marker *pWOX5:GFP*, it was shown from different individuals that *fbl17-1* primary root tips exhibit supernumerary cells expressing the *pWOX5:GFP* marker. Bars = 50 μm.

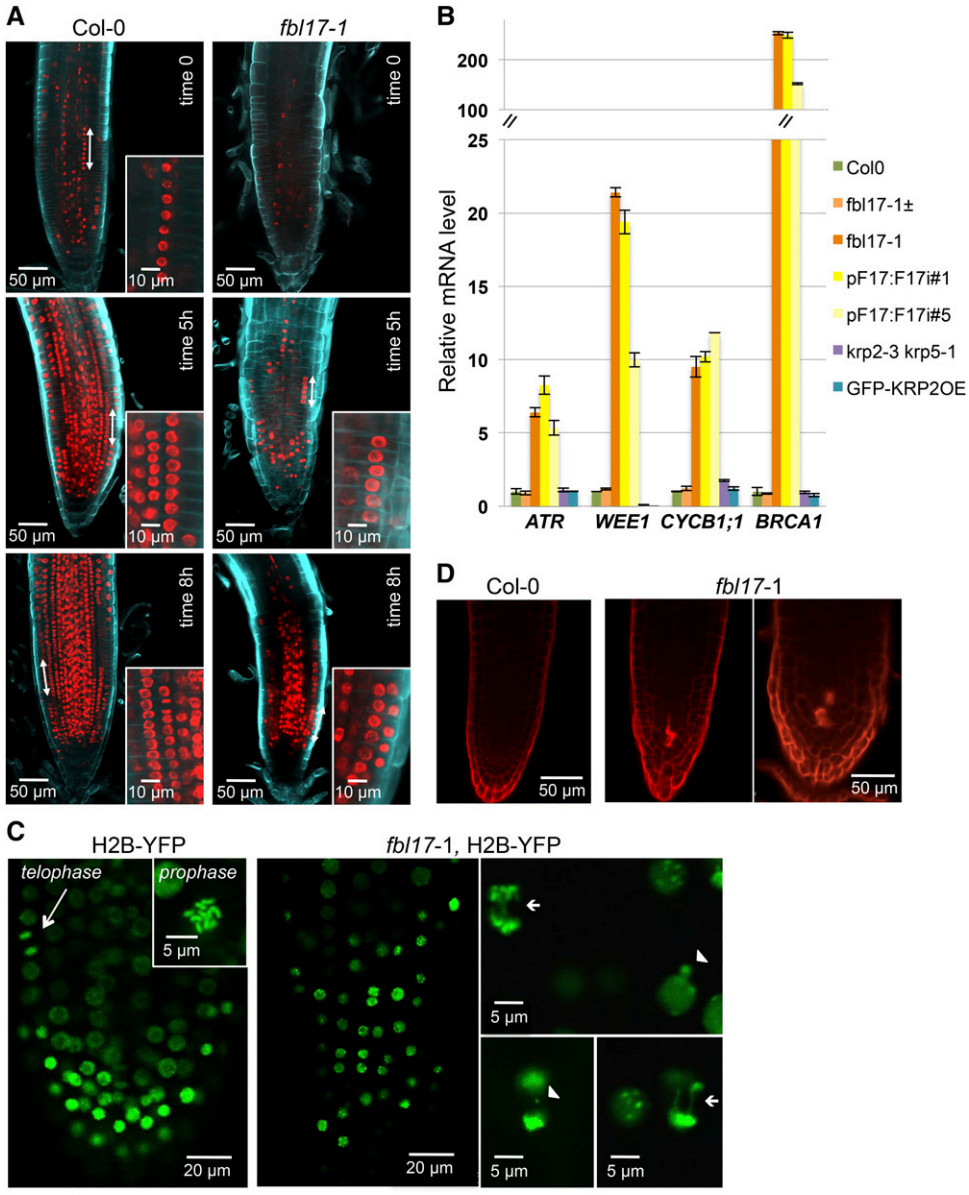

Figure 7. Cells in the *fbl17-1* Root Meristem Exhibit Abnormal Cell Divisions, Leading to the Activation of Cell Cycle Checkpoints.

(A) Observation of nuclei undergoing DNA replication in Arabidopsis Col-0 and *fbl17*-1 mutant primary root tips. Ten-day-old seedlings were incubated for 90 min in MS medium containing 10 µM EdU before root tips were observed by confocal microscopy either directly (time 0) or after further culture in MS liquid (5 and 8 h). To clearly distinguish cell layers, roots were counterstained using Calcofluor. Despite the obvious occurrence of DNA replication in *fbl17-1* root cells revealed by EdU incorporation, synchronized S phase in adjacent cells (double-headed arrow and closeup view), easily seen in wild-type root tips (Hayashi et al., 2013), was barely observed in *fbl17-1*. Bars are as indicated.

(B) Relative expression levels of *ATR*, *WEE1*, *CYCB1;1*, and *BRCA1* transcripts in first pairs of leaves of 20-d-old in vitro-grown plants of the indicated genotypes were determined by quantitative RT-PCR. The bar graph depicts expression level mean values of the indicated transcripts of one independent replicate (±SE of the technical triplicate). The experiment was repeated at least three times, giving the same results.

(C) In mitotic root cells, the nuclear marker H2B-YFP introgressed into wild-type (left panels) and *fbl17-1* mutant (right panels) backgrounds revealed abnormal divisions of some mutant cells, exhibiting chromosome bridges (arrows) or micronucleus formation (arrowheads). In total, 32 primary roots of *fbl17* mutants expressing the H2B-YFP marker were analyzed; 10 of them did not show any mitotic figure, while 22 mitosis events were scored in the remaining plants. Out of these 22 mitosis events, 9 presented lagging chromosomes and/or anaphase bridges. In comparison, among the 20 wild-type root meristems expressing the H2B-YFP marker analyzed, up to 4 mitosis events per root were generally found, and none of the 42 mitosis events observed showed abnormalities. These results indicate that the number of mitosis events occurring in *fbl17* root meristems is not only reduced, but when cells divide, ~40% of them exhibit abnormal chromosome segregation. Bars are as indicated.

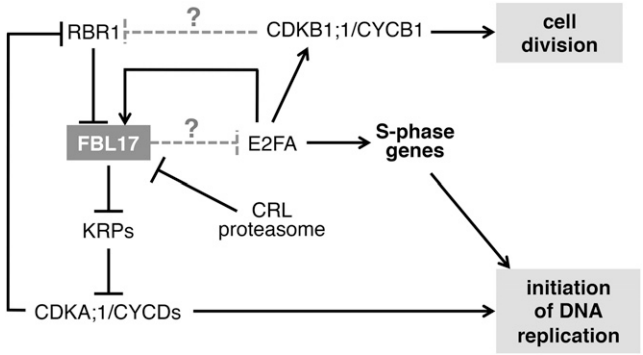

Figure 8. Speculative Model Showing *FBL17* Regulation and Functions in the Control of the Plant Cell Cycle.

FBL17 transcription is positively regulated by the E2FA transcription factor and repressed by RBR1 when it is not phosphorylated by CDKA;1/CYCDs. FBL17 is also regulated at the posttranslational level by the activity of a CRL ubiquitin E3 ligase, targeting it to the proteasome. FBL17 as part of an SCF complex targets KRP proteins for degradation; their overaccumulation blocks CDKA;1 activity and, as a consequence, restrains cell division and plant growth. However, some cells in *fbl17* mutants are still able to enter S phase and even to divide. This process most likely depends on E2FA, which is strongly upregulated in the *fbl17* mutant. Hence, E2FA overaccumulation will induce other genes promoting the S phase as well as CDKB1, which, together with mitotic cyclins, could promote cells to divide. At present, it is unknown whether E2FA is a direct substrate of SCF^{FBL17}.

mitotic divisions (Figure 7C; Supplemental Movies 1A and 1B). However, compared with normal mitotic figures of the wild-type root meristems (Figure 7C), we noted that chromosome segregation was abnormal in some *fbl17* cells, with the presence of lagging chromosomes or anaphase bridges (Figure 7C). Time-lapse recordings of cell division in *fbl17-1* root meristems further supported chromosome missegregation and even micronucleus formation, supporting the evidence of aneuploidy (Supplemental Movies 1A and 1B). Most likely as a consequence of genome instability occurring in those mutant cells, propidium iodide staining of root tips revealed an incidence of cell death (Figure 7D).

DISCUSSION

FBL17 Is the Main Arabidopsis F-Box Protein Involved in Cell Cycle Regulation and Shares Some Functional Similarities with the Mammalian SKP2

In this work, we identified FBL17 as an essential Arabidopsis F-box protein required to maintain normal cell proliferation at all developmental stages investigated. In many respects, FBL17 mirrors the mammalian F-box protein SKP2, which, as part of an SCF ubiquitin E3 ligase complex, targets several cell cycle regulatory proteins (Frescas and Pagano, 2008). For instance, transcription of mammalian *SKP2* is cell cycle regulated, being induced by the transcription factor E2F (Zhang and Wang, 2006). Similarly, Arabidopsis *FBL17* expression is increased during S phase in partially synchronized Arabidopsis cells (Menges et al., 2003), and the gene is induced by E2FA/DPA (Gusti et al., 2009) and repressed by RBR1 (Zhao et al., 2012). Mammalian SKP2 protein is also regulated by the APC/C ubiquitin ligase, triggering its proteasome-dependent degradation (Bashir et al., 2004). Our work also demonstrated posttranslational regulation of Arabidopsis FBL17, although the E3 ubiquitin ligase involved in this process is unknown at present. Finally, SCF^{SKP2} and SCF^{FBL17} promote the degradation of animal and plant CKIs, respectively (Yu et al., 1998; Carrano et al., 1999; Sutterlüty et al., 1999; Tsvetkov et al., 1999; Kim et al., 2008a; Gusti et al., 2009; Zhao et al., 2012; this work).

Mammalian SKP2, however, not only degrades negative regulators of the cell cycle but also positive regulators such as the E2F1 transcription factor (Marti et al., 1999) and the chromatin licensing and DNA replication factor 1 (Cdt1; Li et al., 2003). Despite such an important repertoire of protein targets, mice that are deficient in *SKP2* function are still viable, although with an overall reduced body size attributed to the lack of CKI protein degradation (Nakayama et al., 2004). The viability of the mutant most likely results from the action of other classes of ubiquitin E3 ligases that redundantly target several of these cell cycle substrates. For instance, in mammalian cells, the RING-finger protein KPC1 (Kip1 ubiquitylation-promoting complex1) promotes the degradation of $p27^{Kip1}$ in the cytoplasm in a phosphorylation-independent manner during G1 phase (Kamura et al., 2004), while the $CRL4^{Cdt2}$ (CUL4-DDB1-Cdt2) ubiquitin E3 ligase is in charge of $p21^{Cip1}$ turnover during S phase and also after DNA damage in both *Caenorhabditis elegans* and human cells (Abbas et al., 2008; Kim et al., 2008b). $CRL4^{Cdt2}$ also ubiquitylates the chromatin licensing factor Cdt1 when it interacts on chromatin with proliferating cell nuclear antigen (Havens and Walter, 2011).

In Arabidopsis, while the role of CUL4 in cell cycle regulation is still unclear (Marrocco et al., 2010), our results indicate that FBL17 plays a prominent role in this process. Hence, in comparison with the rather mild phenotype observed in mice lacking *SKP2* (Nakayama et al., 2004), the loss of function of Arabidopsis *FBL17* appears more severe, as only a small proportion of mutants are able to complete their development through flowering and, even so, remain sterile. Although further experiments will be necessary to reveal the full repertoire of SCF^{FBL17} cell cycle substrates, the overall decrease in cell proliferation observed in the *FBL17*-deficient mutants is likely the consequence of impaired KRP protein degradation. Consistent with

Figure 7. (continued).

(D) Spontaneous cell death is revealed by propidium iodide staining in primary root tips of 12-d-old *fbl17-1* mutant seedlings grown in vitro. Two independent experiments were performed, and for each, eight *fbl17* null mutants were stained with propidium iodide. Out of the 16 plants, 13 showed a similar cell death phenotype, while this was never observed in wild-type or *fbl17* heterozygous mutant plants. Bars are as indicated.

such a scenario, the strong KRP accumulation in *fbl17*, as shown for KRP2 (Figure 2G), is expected to downregulate CDKA;1 activity and could explain why *fbl17* loss-of-function mutants resemble the *cdka;1* null mutant (Nowack et al., 2012). However, *fbl17* mutants also exhibit characteristics that cannot be explained by the sole overaccumulation of KRP proteins (see below).

FBL17 Loss of Function Triggers Multiple Cell Cycle Defects and Suppresses Endoreplication

Although loss of *FBL17* causes multiple cell cycle defects, our results suggest that a failure in entering and/or progressing in replication could be the primary cause of the mutant phenotype. First, this is supported by a high content of cells at G0 or G1 stage in all *fbl17* tissues analyzed (Figures 3A, 3B, and 6B) and by the reduced number of EdU-labeled S-phase cells in mutant root meristems (Figure 7A). Second, the high proportion of intermediate 2-4C DNA content could reflect partial DNA replication in the mutant, although we cannot exclude that this material could also correspond to multiple replication rounds of smaller genomic regions, especially those arising from abnormal cell divisions. Third, DNA replication stress induces the expression of checkpoint kinases (Harper and Elledge, 2007; Cools and De Veylder, 2009), and such an induction was observed in *fbl17* null mutants (Figure 7B). Finally, the most striking phenotype of *fbl17* is the lack of endoreplication, a process in which cells repeatedly replicate their DNA without dividing, leading to cellular polyploidy (Breuer et al., 2010). At the molecular level, these defects in observed replication and endoreplication might be the consequence of a failure of *fbl17* mutants to degrade KRP proteins. Hence, it is known that high expression of some of these CKIs, such as KRP1 and KRP2, inhibits endoreplication in postmitotic cells, most likely by blocking S-phase CDK activity (De Veylder et al., 2001; Schnittger et al., 2003; Verkest et al., 2005a). Consistent with this idea, our strong *KRP2*-overexpressing line also showed reduced endoreplication, at least in cotyledons and leaves (Figures 3A and 3B). However, strong *KRP2*-overexpressing lines neither exhibit a higher proportion of the 2-4C DNA content nor induce replication stress checkpoint genes (Figure 7B). Thus, the direct or indirect accumulation of other cell cycle proteins in *fbl17* mutants might explain the stronger phenotype of these plants. Indeed, the upregulation of numerous cell cycle genes in *fbl17* was not expected and was never observed in strong *KRP2*-overexpressing plants (Figure 4). Among these genes, *E2FA*, for which expression is strongly induced in *fbl17*, is of particular interest. Hence, while moderate expression of *E2FA* promotes endoreplication, strong ectopic overexpression of *E2FA* deregulates both cell proliferation and endoreplication (De Veylder et al., 2002). Moreover, a recent work suggests that E2FA in complex with RBR1 (also induced in *fbl17*) prevents entry into endoreplication in proliferating cells (Magyar et al., 2012).

It will be interesting to test whether E2FA is a direct target of FBL17 (Figure 8), a situation that would be reminiscent of mammalian SKP2 (Marti et al., 1999). In such a scenario, E2FA accumulation in the absence of *FBL17* would trigger the activation of a number of genes promoting S-phase entry and also the activation of CDKB1;1 (Boudolf et al., 2004), which, if associated with mitotic cyclins, could promote some cells to divide. However, at least in the root, those cells entering mitosis exhibit abnormalities such as chromosome missegregation that would lead to genome instability and the activation of cell cycle checkpoint responses. Hence, *FBL17* loss-of-function mutants exhibit strong induction of genes responding to both DNA replication stress, such as *ATR1*, *WEE1*, and *CYCB1;1* (Culligan et al., 2004; De Schutter et al., 2007), and DNA double-strand breaks, such as *BRCA1* (Lafarge and Montané, 2003; Reidt et al., 2006). Further experiments will be necessary not only to reveal the full repertoire of SCF^{FBL17} substrates but also to elucidate whether this ubiquitin E3 ligase participates only in cell cycle regulation or is also involved in processes more directly linked to the maintenance of genome stability.

METHODS

Plant Materials

All *Arabidopsis thaliana* T-DNA insertion lines used in the study are described in Supplemental Methods. Primers used for PCR-based genotyping of those lines are listed in Supplemental Table 2. The generation of transgenic lines and primers (Supplemental Table 3) designed for this purpose is described in Supplemental Methods.

Plant Growth Conditions

For in vitro culture conditions, seeds were surface-sterilized using the ethanol method, sown on MES-buffered Murashige and Skoog (MS) medium containing 1× MS salts (Duchefa), 0.8% or 1% (w/v) agar (Fluka), and 1% (w/v) sucrose, pH adjusted to 5.7 with KOH, in the presence of a selective agent when appropriate. Plated seeds were stratified at 4°C for 2 to 3 d and then transferred to a plant growth chamber under a 16-h-light/8-h-dark cycle (22/20°C). The frequency of *fbl17* homozygous mutants in segregating populations was scored from plants cultured on soil. Seeds were stratified on soil at 4°C for 2 to 3 d before being transferred to the greenhouse and kept under a 16-h-light/8-h-dark photoperiod (20/16°C, 70% humidity).

Quantitative RT-PCR

The purification of total RNA from the first pair of leaves of 20-d-old seedlings grown under in vitro conditions was performed using the RNeasy Plant Mini Kit (Qiagen). cDNA was prepared using the High Capacity cDNA Reverse Transcription Kit (Applied Biosystems). Real-time amplification was performed using gene-specific primers and SYBR Green Master Mix (Roche) on a LightCycler LC480 apparatus (Roche) according to the manufacturer's instructions. The mean value of three replicates was normalized using the *EXP* (*AT4G26410*) and *TIP4.1* (*AT4G34270*) genes as internal controls. All primers used in quantitative RT-PCR are listed in Supplemental Table 4.

Ploidy Level Measurement

Nuclear DNA content was measured using the CyStain UV Precise P Kit (Partec) according to the manufacturer's instructions. Nuclei from the first pair of leaves, cotyledon pairs, or the root system of 20-d-old seedlings grown under in vitro conditions were released in nuclei extraction buffer (Partec) by lightly chopping the material with a razor blade, stained with 4′,6-diamidino-2-phenylindole buffer, and filtered through a Celltrics

30-μm mesh (Partec). Between 12,000 and 20,000 isolated nuclei were used for each ploidy level measurement using the Attune Cytometer and the Attune Cytometer software (Life Technologies) recording the relative fluorescence intensities. Flow cytometry experiments were repeated at least three times with leaf samples and two times with cotyledon and root samples using independent biological replicates.

Histology and Light Microscopy Analyses

Histochemical GUS staining was performed as described by Capron et al. (2003). Imaging was performed using the Imager Z-1 microscope (Zeiss) or the Nikon800 microscope. Stomatal index [i.e., stomatal density/(stomatal density + epidermal cell density)] was scored as described by Baerenfaller et al. (2012). Imaging of the epidermal imprints was performed using the Imager Z-1 microscope (Zeiss). For leaf area measurements and scoring of primary root length from the root tip to the root/hypocotyl transition, digital images were captured and processed using ImageJ 1.37 (http://rsbweb.nih.gov/ij/). Cell size measurement was performed on the epidermal imprint images using ImageJ 1.45s (http://rsbweb.nih.gov/ij/).

Confocal Microscopy Analyses and Image Treatments

All confocal microscopy observations were performed by using the LSM 780 microscope (Zeiss). Roots of seedlings expressing fluorescent reporter constructs grown under in vitro conditions were either directly observed or treated with 100 μM MG132 (Sigma-Aldrich) or 25 μM MLN-4924 (Active BioChem) for 6 h and/or counterstained in a solution of 75 μg/mL propidium iodide (Fluka) when indicated. For H2B-YFP signal imaging in living roots expressing the fluorescent marker, confocal images were taken as a consecutive series along the z-axis using the LSM 780 microscope. For H2B-YFP signal imaging in trichome nuclei, microscope settings were kept the same for image acquisition of each genotype, and YFP fluorescence was quantified by measuring the integrated YFP signal density and subtraction of the background fluorescence using the ImageJ 1.37 software (http://rsbweb.nih.gov/ij/). To score cell death, 12-d-old seedlings grown under in vitro conditions were treated as described by Alassimone et al. (2010). For EdU incorporation assays, 9-d-old seedlings grown on solid MS medium were transferred into liquid MS medium overnight for acclimatization. At day 10, EdU (Click-iT EdU Imaging Kit; Invitrogen) was added to the medium at a final concentration of 10 μM. After 90 min of incubation in EdU, samples were prepared according to the manufacturer's instructions either directly or 5 and 8 h after re-incubation in MS liquid medium without EdU. Prior to confocal imaging, root samples were incubated for counterstaining in Calcofluor solution for at least 1 h at room temperature.

Scanning Electron Microscopy

Fresh plant material (i.e., the first pair of leaves of 20-d-old seedlings grown under in vitro culture conditions for trichomes and adaxial epidermis surface and inflorescence for anthers and stigmas) was used for scanning electron microscopy observations. Images were taken using the Tabletop Microscope TM-1000 (Hitachi).

Protein Extraction and Immunoblotting

Total proteins were extracted from the first pair of leaves of 20-d-old seedlings grown under in vitro conditions using denaturating buffer as described by Büche et al. (2000). Total protein extracts (10 or 15 μg) were separated on SDS-PAGE gels and blotted onto Immobilon-P membrane (Millipore). Proteins were detected by using anti-KRP2 antibodies (Verkest et al., 2005a) diluted at 1:1000 (v/v), and Coomassie Brilliant Blue staining was used as a loading control.

Accession Numbers

Sequence data from this article can be found in the Arabidopsis Genome Initiative under the following accession numbers: *FBL17* (At3g54650), *ICK2/KRP2* (At3g50630), *ICK6/KRP3* (At5g48820), *ICK3/KRP5* (At3g24810), and *ICK5/KRP7* (At1g49620).

Supplemental Data

Supplemental Figure 1. Diagram of the genomic locus of *FBL17*.

Supplemental Figure 2. *fbl17* null mutant plants are able to flower, but remained fully sterile.

Supplemental Figure 3. Generation of transgenic *FBL17* knockdown lines using RNA interference.

Supplemental Figure 4. *FBL17* loss of function results in supernumerary QC cells in root tip.

Supplemental Figure 5. *pCYCB1;1:Dbox-GUS* expression level is upregulated in *FBL17*-deficient lines.

Supplemental Figure 6. *FBL17* loss-of-function root cells exhibit altered nucleus size and shape.

Supplemental Table 1. Frequency of homozygous *fbl17* mutants in the progeny of the indicated parental genotypes.

Supplemental Table 2. Primer combinations used for the genotyping of the T-DNA insertion lines.

Supplemental Table 3. Primer combinations used for cloning.

Supplemental Table 4. Primer combinations used for the quantitative RT-PCR analyses.

Supplemental Methods. Plant materials; generation of Arabidopsis transgenic lines; nucleus size and shape estimation.

Supplemental Movie 1. H2B-YFP signal imaging in *fbl17* living roots revealed chromosome missegregation.

ACKNOWLEDGMENTS

We thank Christian Luschnig (BOKU, Vienna) for providing *krp* mutant lines, Freddy Barnèche (ENS) for the *H2B-YFP* construct, B. Scheres (Wageningen University) for the GUS-expressing QC46 line, and Masaki Ito (Nagoya University) for providing stomata reporter lines. This work was supported by the Agence Nationale de la Recherche (Grants ANR 2011 and BSV2 027 02 to K. Marrocco and K. Masoud) and by the European Regional Development Fund (grant to A. Thomann) in the framework of INTERREG IV for cofinancing the Trinational Institute for Plant Research, to which the Institut de Biologie Moléculaire des Plantes belongs.

AUTHOR CONTRIBUTIONS

K. Marrocco, A.T., and S.N. developed and carried out the genetic approach. K. Marrocco and A.G. generated transgenic lines. K. Marrocco, M.B., and S.N. performed plant development characterizations and immunoblot analyses. S.N., K. Marrocco, and K. Masoud performed quantitative PCR analyses, light microscopy analyses, and scanning and laser confocal imaging. S.N. performed flow cytometry analyses. P.G. conceived and supervised the study with input from S.N. and A.S. P.G. and S.N. wrote the article.

Received December 11, 2014; revised March 31, 2015; accepted April 11, 2015; published May 5, 2015.

REFERENCES

Abbas, T., Sivaprasad, U., Terai, K., Amador, V., Pagano, M., and Dutta, A. (2008). PCNA-dependent regulation of p21 ubiquitylation and degradation *via* the CRL4^{Cdt2} ubiquitin ligase complex. Genes Dev. **22:** 2496–2506.

Alassimone, J., Naseer, S., and Geldner, N. (2010). A developmental framework for endodermal differentiation and polarity. Proc. Natl. Acad. Sci. USA **107:** 5214–5219.

Baerenfaller, K., et al. (2012). Systems-based analysis of Arabidopsis leaf growth reveals adaptation to water deficit. Mol. Syst. Biol. **8:** 606.

Bashir, T., Dorrello, N.V., Amador, V., Guardavaccaro, D., and Pagano, M. (2004). Control of the SCF$^{Skp2\text{-}Cks1}$ ubiquitin ligase by the APC/C^{Cdh1} ubiquitin ligase. Nature **428:** 190–193.

Bass, H.W., Wear, E.E., Lee, T.J., Hoffman, G.G., Gumber, H.K., Allen, G.C., Thompson, W.F., and Hanley-Bowdoin, L. (2014). A maize root tip system to study DNA replication programmes in somatic and endocycling nuclei during plant development. J. Exp. Bot. **65:** 2747–2756.

Blilou, I., Xu, J., Wildwater, M., Willemsen, V., Paponov, I., Friml, J., Heidstra, R., Aida, M., Palme, K., and Scheres, B. (2005). The PIN auxin efflux facilitator network controls growth and patterning in Arabidopsis roots. Nature **433:** 39–44.

Boudolf, V., Vlieghe, K., Beemster, G.T., Magyar, Z., Torres Acosta, J.A., Maes, S., Van Der Schueren, E., Inzé, D., and De Veylder, L. (2004). The plant-specific cyclin-dependent kinase CDKB1;1 and transcription factor E2Fa-DPa control the balance of mitotically dividing and endoreduplicating cells in *Arabidopsis*. Plant Cell **16:** 2683–2692.

Bramsiepe, J., Wester, K., Weinl, C., Roodbarkelari, F., Kasili, R., Larkin, J.C., Hülskamp, M., and Schnittger, A. (2010). Endoreplication controls cell fate maintenance. PLoS Genet. **6:** e1000996.

Breuer, C., Ishida, T., and Sugimoto, K. (2010). Developmental control of endocycles and cell growth in plants. Curr. Opin. Plant Biol. **13:** 654–660.

Büche, C., Poppe, C., Schäfer, E., and Kretsch, T. (2000). eid1: A new *Arabidopsis* mutant hypersensitive in phytochrome A-dependent high-irradiance responses. Plant Cell **12:** 547–558.

Capron, A., Serralbo, O., Fülöp, K., Frugier, F., Parmentier, Y., Dong, A., Lecureuil, A., Guerche, P., Kondorosi, E., Scheres, B., and Genschik, P. (2003). The *Arabidopsis* anaphase-promoting complex or cyclosome: Molecular and genetic characterization of the APC2 subunit. Plant Cell **15:** 2370–2382.

Carrano, A.C., Eytan, E., Hershko, A., and Pagano, M. (1999). SKP2 is required for ubiquitin-mediated degradation of the CDK inhibitor p27. Nat. Cell Biol. **1:** 193–199.

Churchman, M.L., et al. (2006). SIAMESE, a plant-specific cell cycle regulator, controls endoreplication onset in *Arabidopsis thaliana*. Plant Cell **18:** 3145–3157.

Cools, T., and De Veylder, L. (2009). DNA stress checkpoint control and plant development. Curr. Opin. Plant Biol. **12:** 23–28.

Culligan, K., Tissier, A., and Britt, A. (2004). ATR regulates a G2-phase cell-cycle checkpoint in *Arabidopsis thaliana*. Plant Cell **16:** 1091–1104.

Culligan, K.M., Robertson, C.E., Foreman, J., Doerner, P., and Britt, A.B. (2006). ATR and ATM play both distinct and additive roles in response to ionizing radiation. Plant J. **48:** 947–961.

De Schutter, K., Joubès, J., Cools, T., Verkest, A., Corellou, F., Babiychuk, E., Van Der Schueren, E., Beeckman, T., Kushnir, S., Inzé, D., and De Veylder, L. (2007). *Arabidopsis* WEE1 kinase controls cell cycle arrest in response to activation of the DNA integrity checkpoint. Plant Cell **19:** 211–225.

De Veylder, L., Beeckman, T., Beemster, G.T., Krols, L., Terras, F., Landrieu, I., van der Schueren, E., Maes, S., Naudts, M., and Inzé, D. (2001). Functional analysis of cyclin-dependent kinase inhibitors of *Arabidopsis*. Plant Cell **13:** 1653–1668.

De Veylder, L., Beeckman, T., Beemster, G.T.S., de Almeida Engler, J., Ormenese, S., Maes, S., Naudts, M., Van Der Schueren, E., Jacqmard, A., Engler, G., and Inzé, D. (2002). Control of proliferation, endoreduplication and differentiation by the *Arabidopsis* E2Fa-DPa transcription factor. EMBO J. **21:** 1360–1368.

Dissmeyer, N., Weimer, A.K., Pusch, S., De Schutter, K., Alvim Kamei, C.L., Nowack, M.K., Novak, B., Duan, G.L., Zhu, Y.G., De Veylder, L., and Schnittger, A. (2009). Control of cell proliferation, organ growth, and DNA damage response operate independently of dephosphorylation of the *Arabidopsis* Cdk1 homolog CDKA;1. Plant Cell **21:** 3641–3654.

Donnelly, P.M., Bonetta, D., Tsukaya, H., Dengler, R.E., and Dengler, N.G. (1999). Cell cycling and cell enlargement in developing leaves of Arabidopsis. Dev. Biol. **215:** 407–419.

Frescas, D., and Pagano, M. (2008). Deregulated proteolysis by the F-box proteins SKP2 and beta-TrCP: Tipping the scales of cancer. Nat. Rev. Cancer **8:** 438–449.

Galan, J.M., and Peter, M. (1999). Ubiquitin-dependent degradation of multiple F-box proteins by an autocatalytic mechanism. Proc. Natl. Acad. Sci. USA **96:** 9124–9129.

Genschik, P., Marrocco, K., Bach, L., Noir, S., and Criqui, M.-C. (2014). Selective protein degradation: A rheostat to modulate cell-cycle phase transitions. J. Exp. Bot. **65:** 2603–2615.

Gusti, A., Baumberger, N., Nowack, M., Pusch, S., Eisler, H., Potuschak, T., De Veylder, L., Schnittger, A., and Genschik, P. (2009). The *Arabidopsis thaliana* F-box protein FBL17 is essential for progression through the second mitosis during pollen development. PLoS ONE **4:** e4780.

Hakenjos, J.P., Richter, R., Dohmann, E.M., Katsiarimpa, A., Isono, E., and Schwechheimer, C. (2011). MLN4924 is an efficient inhibitor of NEDD8 conjugation in plants. Plant Physiol. **156:** 527–536.

Harashima, H., Dissmeyer, N., and Schnittger, A. (2013). Cell cycle control across the eukaryotic kingdom. Trends Cell Biol. **23:** 345–356.

Harper, J.W., and Elledge, S.J. (2007). The DNA damage response: Ten years after. Mol. Cell **28:** 739–745.

Havens, C.G., and Walter, J.C. (2011). Mechanism of CRL4(Cdt2), a PCNA-dependent E3 ubiquitin ligase. Genes Dev. **25:** 1568–1582.

Hayashi, K., Hasegawa, J., and Matsunaga, S. (2013). The boundary of the meristematic and elongation zones in roots: Endoreduplication precedes rapid cell expansion. Sci. Rep. **3:** 2723.

Helariutta, Y., Fukaki, H., Wysocka-Diller, J., Nakajima, K., Jung, J., Sena, G., Hauser, M.T., and Benfey, P.N. (2000). The SHORT-ROOT gene controls radial patterning of the Arabidopsis root through radial signaling. Cell **101:** 555–567.

Inzé, D., and De Veylder, L. (2006). Cell cycle regulation in plant development. Annu. Rev. Genet. **40:** 77–105.

Johnson, A., and Skotheim, J.-M. (2013). Start and the restriction point. Curr. Opin. Cell Biol. **25:** 717–723.

Kamura, T., Hara, T., Matsumoto, M., Ishida, N., Okumura, F., Hatakeyama, S., Yoshida, M., Nakayama, K., and Nakayama, K.I. (2004). Cytoplasmic ubiquitin ligase KPC regulates proteolysis of p27^{Kip1} at G1 phase. Nat. Cell Biol. **6:** 1229–1235.

Kim, H.J., Oh, S.A., Brownfield, L., Hong, S.H., Ryu, H., Hwang, I., Twell, D., and Nam, H.G. (2008a). Control of plant germline proliferation by SCF^{FBL17} degradation of cell cycle inhibitors. Nature **455:** 1134–1137.

Kim, Y., Starostina, N.G., and Kipreos, E.T. (2008b). The CRL4^{Cdt2} ubiquitin ligase targets the degradation of p21^{Cip1} to control replication licensing. Genes Dev. **22:** 2507–2519.

Lafarge, S., and Montané, M.H. (2003). Characterization of *Arabidopsis thaliana* ortholog of the human breast cancer susceptibility gene 1: AtBRCA1, strongly induced by gamma rays. Nucleic Acids Res. **31:** 1148–1155.

Li, X., Zhao, Q., Liao, R., Sun, P., and Wu, X. (2003). The SCF^{Skp2} ubiquitin ligase complex interacts with the human replication licensing factor Cdt1 and regulates Cdt1 degradation. J. Biol. Chem. **278:** 30854–30858.

Liu, J., et al. (2008). Targeted degradation of the cyclin-dependent kinase inhibitor ICK4/KRP6 by RING-type E3 ligases is essential for mitotic cell cycle progression during *Arabidopsis* gametogenesis. Plant Cell **20:** 1538–1554.

Magyar, Z., Horváth, B., Khan, S., Mohammed, B., Henriques, R., De Veylder, L., Bakó, L., Scheres, B., and Bögre, L. (2012). Arabidopsis E2FA stimulates proliferation and endocycle separately through RBR-bound and RBR-free complexes. EMBO J. **31:** 1480–1493.

Marrocco, K., Bergdoll, M., Achard, P., Criqui, M.C., and Genschik, P. (2010). Selective proteolysis sets the tempo of the cell cycle. Curr. Opin. Plant Biol. **13:** 631–639.

Marti, A., Wirbelauer, C., Scheffner, M., and Krek, W. (1999). Interaction between ubiquitin-protein ligase SCF^{SKP2} and E2F-1 underlies the regulation of E2F-1 degradation. Nat. Cell Biol. **1:** 14–19.

Menges, M., Hennig, L., Gruissem, W., and Murray, J.A.H. (2003). Genome-wide gene expression in an Arabidopsis cell suspension. Plant Mol. Biol. **53:** 423–442.

Murray, A.W. (2004). Recycling the cell cycle: Cyclins revisited. Cell **116:** 221–234.

Nadeau, J.A., and Sack, F.D. (2002). Control of stomatal distribution on the Arabidopsis leaf surface. Science **296:** 1697–1700.

Nakayama, K., Nagahama, H., Minamishima, Y.A., Miyake, S., Ishida, N., Hatakeyama, S., Kitagawa, M., Iemura, S., Natsume, T., and Nakayama, K.I. (2004). Skp2-mediated degradation of p27 regulates progression into mitosis. Dev. Cell **6:** 661–672.

Nowack, M.K., Harashima, H., Dissmeyer, N., Zhao, X., Bouyer, D., Weimer, A.K., De Winter, F., Yang, F., and Schnittger, A. (2012). Genetic framework of cyclin-dependent kinase function in Arabidopsis. Dev. Cell **22:** 1030–1040.

Nurse, P. (2000). A long twentieth century of the cell cycle and beyond. Cell **100:** 71–78.

Peres, A., et al. (2007). Novel plant-specific cyclin-dependent kinase inhibitors induced by biotic and abiotic stresses. J. Biol. Chem. **282:** 25588–25596.

Reidt, W., Wurz, R., Wanieck, K., Chu, H.H., and Puchta, H. (2006). A homologue of the breast cancer-associated gene BARD1 is involved in DNA repair in plants. EMBO J. **25:** 4326–4337.

Sabatini, S., Beis, D., Wolkenfelt, H., Murfett, J., Guilfoyle, T., Malamy, J., Benfey, P., Leyser, O., Bechtold, N., Weisbeek, P., and Scheres, B. (1999). An auxin-dependent distal organizer of pattern and polarity in the Arabidopsis root. Cell **99:** 463–472.

Schnittger, A., Weinl, C., Bouyer, D., Schöbinger, U., and Hülskamp, M. (2003). Misexpression of the cyclin-dependent kinase inhibitor ICK1/KRP1 in single-celled *Arabidopsis* trichomes reduces endoreduplication and cell size and induces cell death. Plant Cell **15:** 303–315.

Schwob, E., Böhm, T., Mendenhall, M.D., and Nasmyth, K. (1994). The B-type cyclin kinase inhibitor p40SIC1 controls the G1 to S transition in *S. cerevisiae*. Cell **79:** 233–244.

Starostina, N.G., and Kipreos, E.T. (2012). Multiple degradation pathways regulate versatile CIP/KIP CDK inhibitors. Trends Cell Biol. **22:** 33–41.

Sutterlüty, H., Chatelain, E., Marti, A., Wirbelauer, C., Senften, M., Müller, U., and Krek, W. (1999). $p45^{SKP2}$ promotes $p27^{Kip1}$ degradation and induces S phase in quiescent cells. Nat. Cell Biol. **1:** 207–214.

Torres Acosta, J.A., Fowke, L.C., and Wang, H. (2011). Analyses of phylogeny, evolution, conserved sequences and genome-wide expression of the ICK/KRP family of plant CDK inhibitors. Ann. Bot. (Lond.) **107:** 1141–1157.

Tsvetkov, L.M., Yeh, K.H., Lee, S.J., Sun, H., and Zhang, H. (1999). $p27^{Kip1}$ ubiquitination and degradation is regulated by the SCF^{Skp2} complex through phosphorylated Thr187 in p27. Curr. Biol. **9:** 661–664.

Verkest, A., Manes, C.L., Vercruysse, S., Maes, S., Van Der Schueren, E., Beeckman, T., Genschik, P., Kuiper, M., Inzé, D., and De Veylder, L. (2005a). The cyclin-dependent kinase inhibitor KRP2 controls the onset of the endoreduplication cycle during *Arabidopsis* leaf development through inhibition of mitotic CDKA;1 kinase complexes. Plant Cell **17:** 1723–1736.

Verkest, A., Weinl, C., Inzé, D., De Veylder, L., and Schnittger, A. (2005b). Switching the cell cycle. Kip-related proteins in plant cell cycle control. Plant Physiol. **139:** 1099–1106.

Welch, D., Hassan, H., Blilou, I., Immink, R., Heidstra, R., and Scheres, B. (2007). Arabidopsis JACKDAW and MAGPIE zinc finger proteins delimit asymmetric cell division and stabilize tissue boundaries by restricting SHORT-ROOT action. Genes Dev. **21:** 2196–2204.

Yu, Z.K., Gervais, J.L., and Zhang, H. (1998). Human CUL-1 associates with the SKP1/SKP2 complex and regulates $p21^{CIP1/WAF1}$ and cyclin D proteins. Proc. Natl. Acad. Sci. USA **95:** 11324–11329.

Zhang, L., and Wang, C. (2006). F-box protein Skp2: A novel transcriptional target of E2F. Oncogene **25:** 2615–2627.

Zhao, X., Harashima, H., Dissmeyer, N., Pusch, S., Weimer, A.K., Bramsiepe, J., Bouyer, D., Rademacher, S., Nowack, M.K., Novak, B., Sprunck, S., and Schnittger, A. (2012). A general G1/S-phase cell-cycle control module in the flowering plant *Arabidopsis thaliana*. PLoS Genet. **8:** e1002847.